

New High Frequency Inverter Topologies Integrated with the Coupled Inductor Bridge Arm

Yihua Hu¹, *Member, IEEE*, Bing Ji², *Member, IEEE*, Stephen Finney¹, Weidong Xiao³, *Senior Member,*

Wengping Cao⁴, *Senior Member, IEEE*

¹ (*Electrical & Electronics Engineering, University of Strathclyde, Glasgow, UK*)

² (*Department of Engineering, University of Leicester, Leicester, UK*)

³ (*Electrical Engineering and Computer Science, Masdar Institute of Science and Technology, UAE*)

⁴ (*Department of Electrical Engineering and Computer Science, Massachusetts Institute of Technology, USA*)

Abstract –A new topology of the high frequency AC (HFAC) inverter bridge arm is proposed which comprises a coupled inductor, a switching device and an active clamp circuit. Based on it, new single-phase and three-phase inverters are proposed and their operating states are analyzed along with the traditional H-bridge inverter. Multi-phase and multi-level isolated inverters are also developed using the HFAC bridge arm. Furthermore, based on the proposed HFAC, a frond-end DC-DC converter is also developed for photovoltaic (PV) systems to demonstrate the application of the proposed HFAC converter. Simulation and experimental results from prototype converters are carried out to validate the proposed topologies which can be utilized widely in high frequency power conversion applications such as induction heating and wireless power transfer.

Index terms –**Bridge arm, coupled inductor, DC-DC converters, inverters, photovoltaics.**

None of the material in this paper has been published or is under consideration for publication elsewhere.

I. INTRODUCTION

High frequency alternating current (HFAC) systems are widely applied for induction heating [1], aerospace [2], vehicles [3], microgrids [4][5], power distribution systems [6]-[8], telecommunication [9], computer power supplies [9] and medium/high voltage gate driving systems [10] owing to their merits of simple transforming structure, low cost and low component count, and effective ground noise isolation [10].

One critical component of HFAC systems is their front-end inverter, which converts DC to HFAC. A common topology for single-phase systems is the H-bridge [2] [see Fig. 1(a)], which is also refers to as the full bridge [10] or the buck inverter [11]. One important feature of the H-bridge is that its input DC voltage is always higher than the average AC voltage. Typically, a boost topology of the DC-AC inverter is needed [11] to step up the voltage output, as illustrated in Fig. 1(b). Sometimes the half bridge is also adopted, of which one switch arm is replaced by capacitor banks [12]. Resonant tanks are specifically designed in [10][13] to add to the H-bridge so as to extend the operating range of soft switching and to minimize the total harmonic distortion (THD) in HFAC systems, as shown in Fig. 1(c). A single-switch resonant inverter topology is proposed in [14] to use LC resonance for AC signal generation. Resonant topologies can also include the asymmetrical pulse-width-modulated (APWM) resonant inverter, which is constructed with two power switches [15][16].

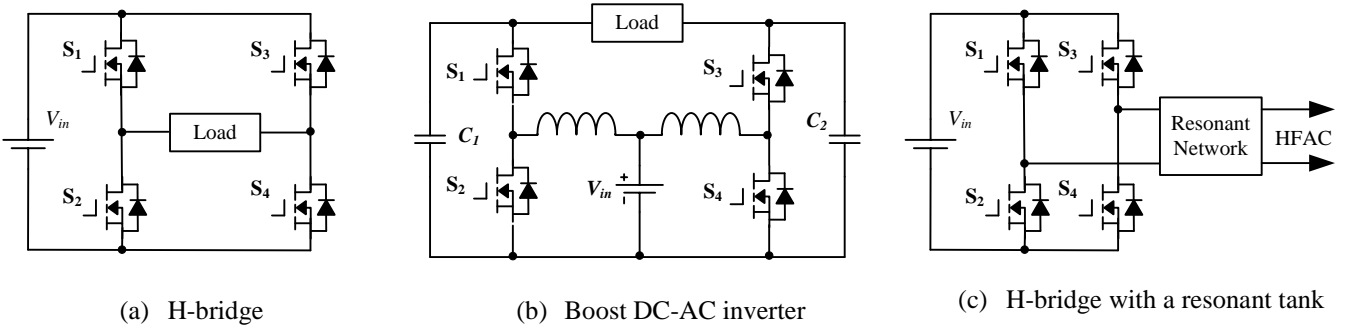


Fig. 1 Common H-bridge inverter topologies.

In the front-end converter, coupled inductors are widely used to achieve high step-up DC-DC conversion, which is particularly important for photovoltaic [17] and fuel cell applications [18]. The same concept can be applied to the HFAC power converter systems. In this paper, a class of new HFAC inverter topologies are proposed for use of single-phase, three-phase, multi-phase, and multi-levels. A coupled inductor bridge arm is integrated in them to achieve soft switching, electrical isolation, and structural flexibility. Their effectiveness is validated by experimental tests on a 400-W prototype.

II. PROPOSED INVERTERS

(a) Single-phase inverter

The traditional H-bridge inverter arm can generate outputs of 0 and $\pm V_{in}$ between the central node, as in Fig. 2(a). It can

be modified by replacing the upper switches with coupled inductors, as shown in Fig. 2(b). This paper proposes a new inverter with active clamp circuits to recover leakage inductance energy and to realize soft switching, as shown in Fig. 2(c). In the figure, S_1 and S_2 are the main switching devices. Two switches S_{c1} , S_{c2} and two clamp capacitors C_{c1} , C_{c2} are employed to form an active clamp circuit to limit the main switch voltage stress and recycle leakage inductance energy. The primary windings of the coupled inductors L_1 and L_2 are used as filter inductors whilst their secondary windings are reverse series connected. The numbers of primary and secondary windings are n_1 and n_2 , respectively, and their turns ratio n is defined as n_2/n_1 . The coupling references are marked as “•” for L_1 , and “*” for L_2 . The leakage inductances are L_{LK1} and L_{LK2} , for L_1 and L_2 , respectively.

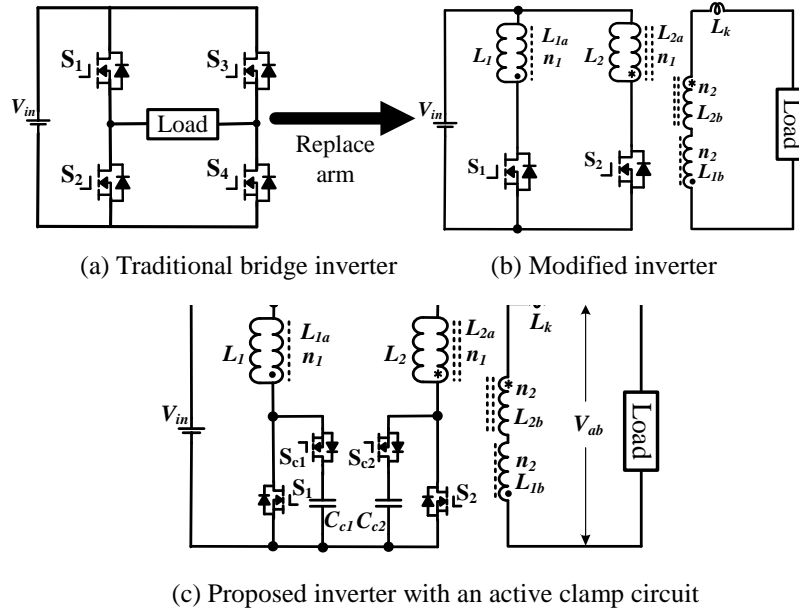


Fig. 2 Traditional and proposed single-phase inverters.

S_1 and S_2 have the same duty ratio as D and a phase shift of Φ . The gate signals for S_1 and S_{c1} are complementary, and so are for S_2 and S_{c2} . Typical waveforms of the single-phase inverter are illustrated in Fig. 3. For comparison of the proposed inverter with the traditional H-bridge inverter, four main operating states of the inverters are studied as follows.

State 1 [t_0 - t_1]: The main switches S_1 and S_2 are both in ON state before t_1 . The two coupled inductors work in the Flyback mode to charge energy from the DC source. The secondary sides of the coupled inductors are equivalent to two reverse series connected DC sources. V_{L2} and V_{L1} and thus the output of the secondary sides is zero, similar to the traditional H-bridge, as shown in Fig. 4(a).

State 2 [t_1 - t_2]: At t_1 , the main switch S_2 turns OFF while S_{c2} turns ON, which reverses its secondary side output. During this state, the coupled inductors L_1 and L_2 operate in the Forward and Flyback modes, respectively, to transfer energy to the load. Fig. 4(b) illustrates the equivalent state of the traditional H-bridge topology for comparison. Due to the active clamp circuit, the main switch voltage stress and the secondary side output voltage are given in (1) and (2), respectively. By Comparison, the voltage stress of the main switches is much lower than the output voltage.

$$V_{DS} = \frac{V_{in}}{1-D} \quad (1)$$

$$\frac{V_{ab}}{V_{in}} = \frac{n}{1-D} \quad (2)$$

State 3 $[t_2-t_3]$: At t_2 , the main switch S_2 turns ON, and the two coupled inductors again work in the Flyback mode to store energy. As in state 1, the secondary side output voltage is zero.

State 4 $[t_3-t_4]$: At t_3 , the main switch S_1 turns OFF and S_{c1} turns ON, which reverses the voltage polarity of the secondary side of the coupled inductor L_1 . During this state, the coupled inductor L_1 and L_2 operate in Flyback and Forward modes, respectively, to transfer energy to the load. Fig. 4(d) illustrates the equivalent state of the traditional H-bridge topology.

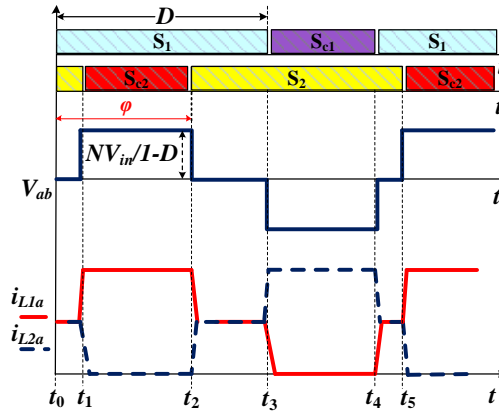


Fig. 3 Output waveforms of the proposed single-phase inverter.

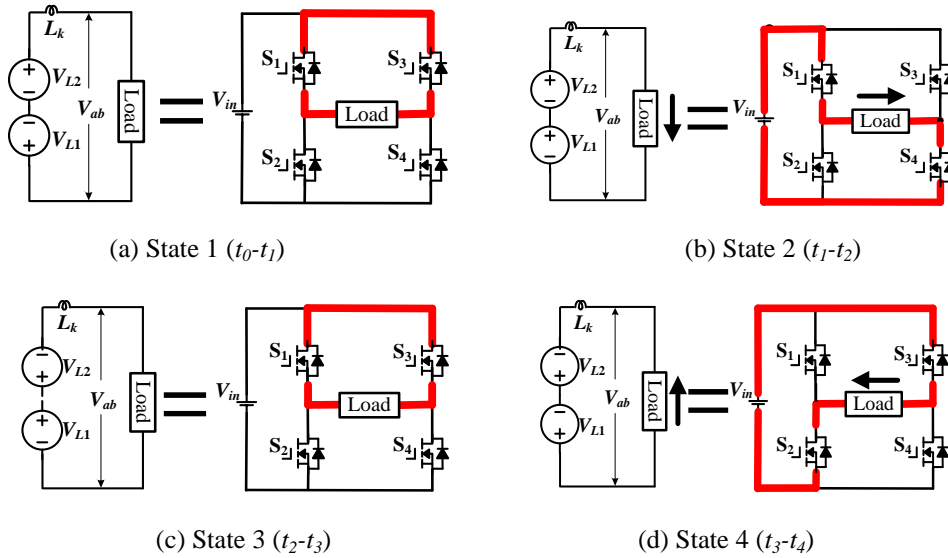


Fig. 4 Operating states of the proposed single-phase inverter

(b) Three-phase inverter

The proposed inverter bridge arm can be built up to form a three-phase inverter. As shown in Fig. 5, the proposed inverter consists of three coupled inductor bridges while their secondary sides are star connected. Its output waveforms and six main operating states are presented in Figs. 6 and 7, respectively. In Fig. 6, V_A , V_B and V_C are the output voltages of the

coupled inductors. Each operating state of the secondary side of the inverter is equivalent to that of the traditional three-phase inverter.

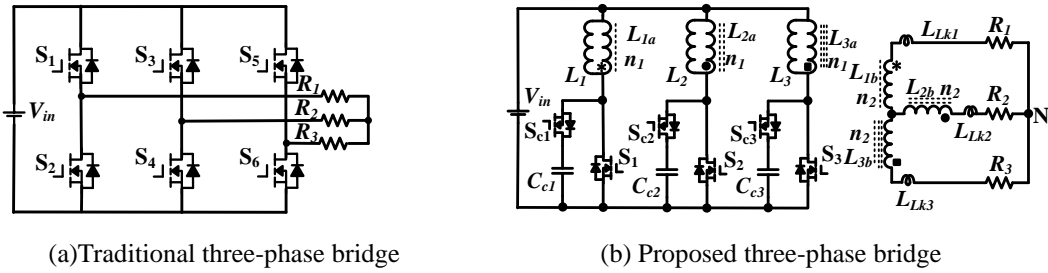


Fig. 5 Traditional and proposed three-phase inverters.

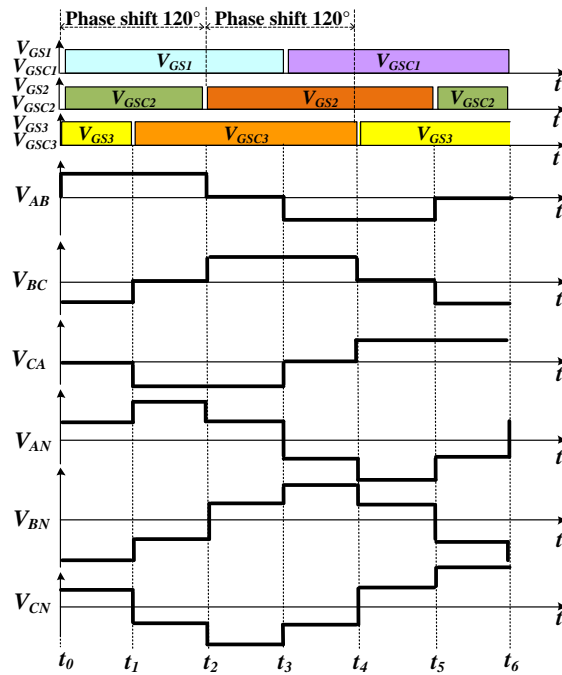
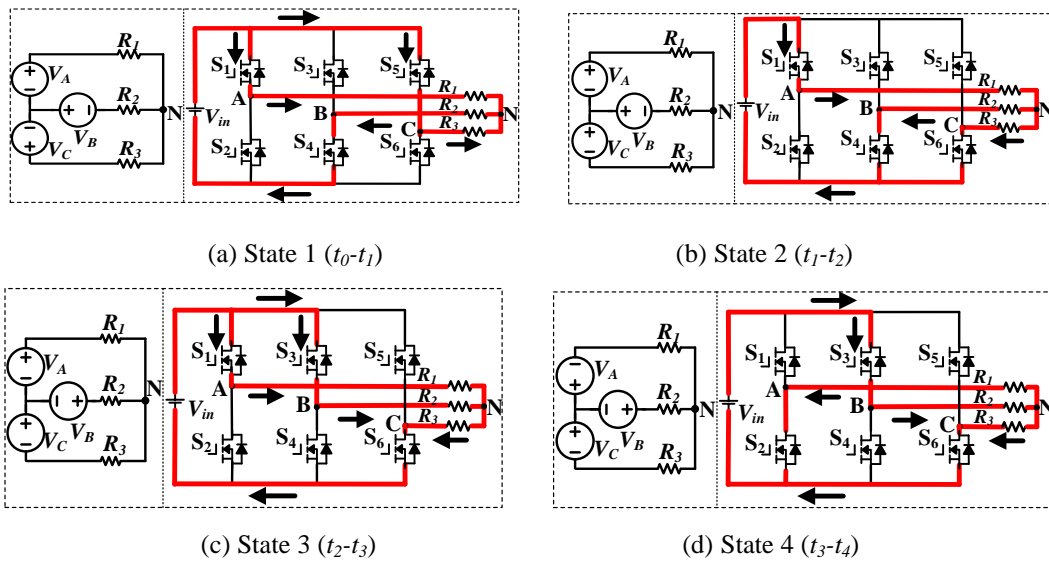


Fig. 6 Output waveforms of the proposed three-phase inverter.



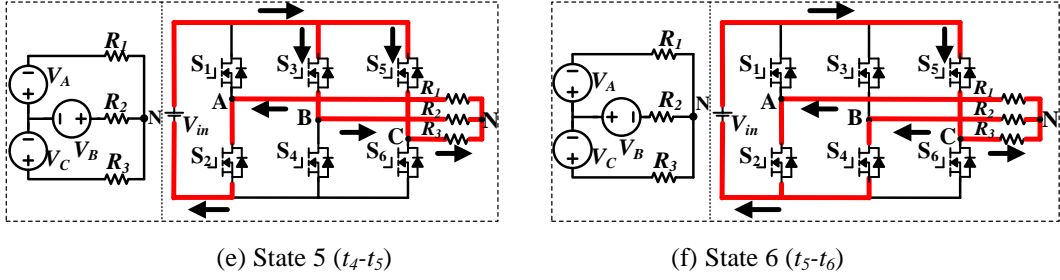


Fig. 7 Six operating states of the proposed three-phase inverter.

(c) *Multi-phase and multi-level topologies*

Similar to the three-phase inverter, any multi-phase inverter can also be constructed using the proposed bridge arm. Fig. 8(a) shows a four-phase inverter topology as an example. Moreover, multi-level inverters (traditional cascaded inverters) can also be derived from the proposed inverter. Fig. 8(b) demonstrates a three-level inverter topology as an example. The difference between the two examples lies in the electrical connection of the secondary side of the coupled inductors where the former is star-connected and the latter connects the two winding pairs a (for inductors 1 and 2) and b (for inductors 3 and 4) in series. The same method can be used to develop inverters with more phases or more output voltage levels. A simulation study is conducted in PSIM environment to evaluate the inverter performance and its results for these multi-phase and multi-level inverters are shown in Fig. 9. In the simulation, the switching frequency is set to 50 kHz, the main switches have a 50% duty ratio over each phase and a phase shift of $T/4$ between one another. In Fig. 9(a), V_{ab} , V_{bc} , V_{cd} , V_{da} are the line voltage, and V_a , V_b , V_c , V_d are the phase voltage. In Fig. 9(b), the switches S_2 , S_3 , S_4 are phase shifted by $T/2$, $T/6$ and $T/3$, respectively. With the phase shift and PWM control of each bridge arm, a multi-level output is achieved and this output voltage is twice of a two-level inverter.

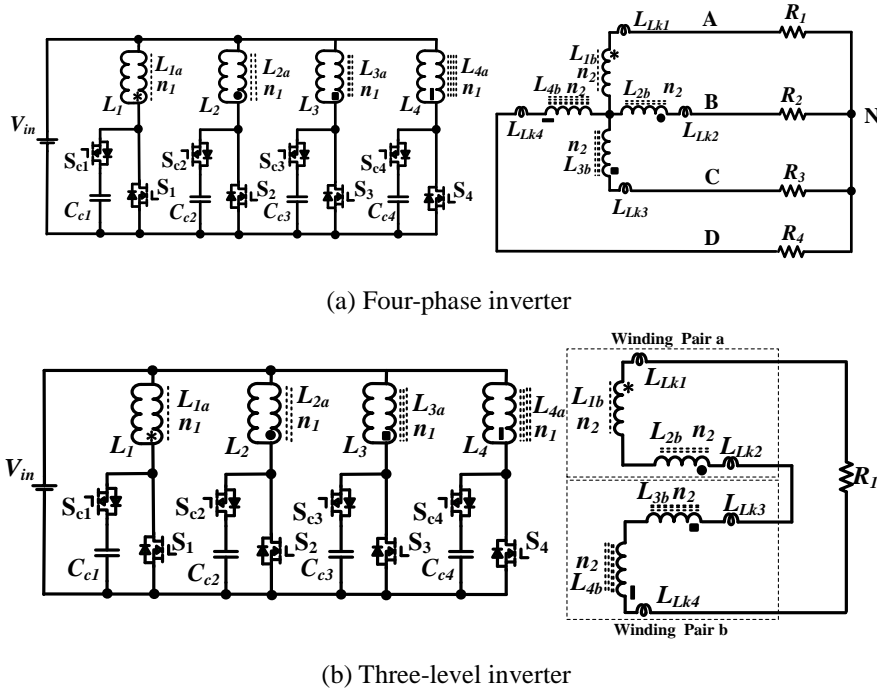
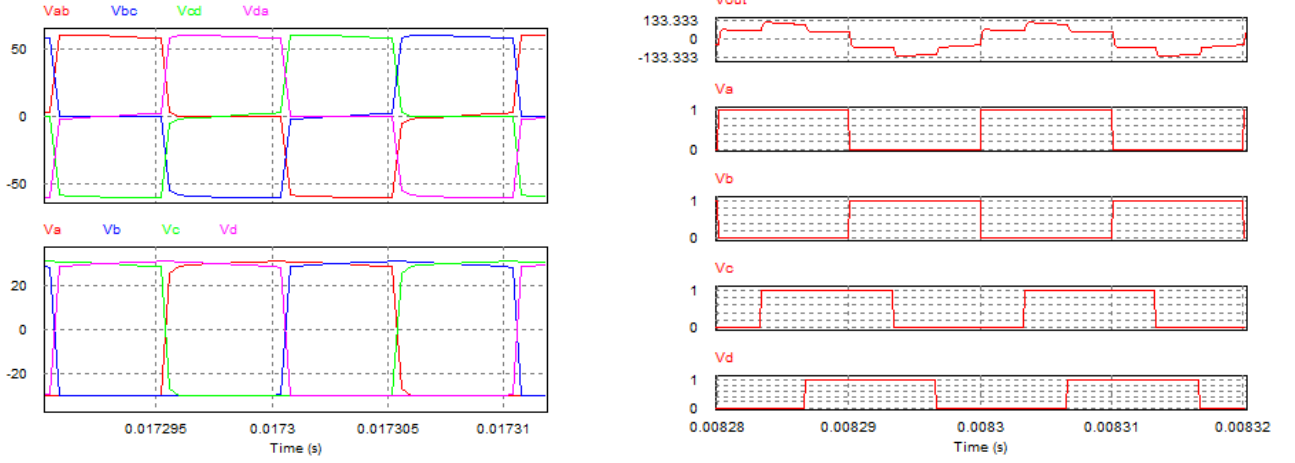


Fig. 8 New topologies derived from the proposed inverter.



(a) Four-phase inverter

(b) Three-level inverter

Fig. 9 Simulation results for multi-phase and multi-level inverters.

III. PROPOSED TOPOLOGIES FOR APPLICATIONS

The proposed inverter can be applied to different applications by combining with different rectifier circuits. Taking photovoltaics (PV) for example, the basic requirements for a front-end DC-DC converter are high step-up ratio and electrical isolation because of the leakage current of PV modules and the low voltage of each module. Fig. 10 presents a topology which includes a three phase inverter (Fig.5 (b)) and a three phase rectifier bridge. The primary side is a parallel connection that decreases the input current ripple while the secondary side is a modular structure and its interleaved working mode can decrease the capacitance of output capacitor. In case one bridge arm is faulted, the topology can still operate with the remaining healthy arms, as shown in Fig. 11 where switching device S1 is broken. Clearly, the bridge arm 1 stops working. On the secondary side, L_{lb} can block the fault so that the proposed topology operates with two bridge arms. The design considerations are as follow:

(1) The primary side switching devices

In the steady-state operation, the voltage stress of the primary power devices is equal to the voltage on the clamp capacitor, as shown in Eq. (3)

$$V_{DS} = V_{DSc} = \frac{V_{in}}{1-D} \quad (3)$$

(2) Clamp capacitor

The energy stored in the magnetizing inductor transfers to the clamping capacitor, the corresponding energy balance can be expressed as

$$C_c = \frac{L_{Lm} \cdot I_{Lm}^2}{V_{Cc\max}^2 - V_{Cc}^2} \quad (4)$$

where $V_{C_{max}}$ is the maximum voltage of clamp capacitor; V_{Cc} is the average voltage of clamp capacitor; L_{Lm} is the excitation inductance of coupled inductor; I_{Lm} is the corresponding current.

(3) Rectifier diode

The voltage stress of rectifier diode is equal to the output voltage.

(4) Turns ratio of the coupled inductor

The duty ratio can be set to the minimum value, and a proper turn ratio is chosen according Eq. (2).

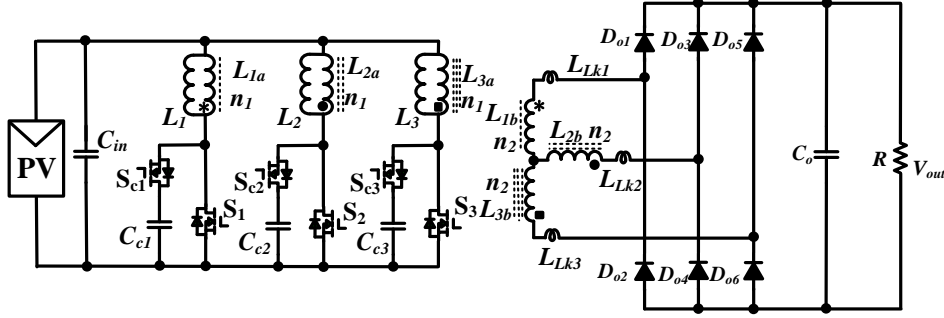


Fig. 10 Front-end topology for PV applications

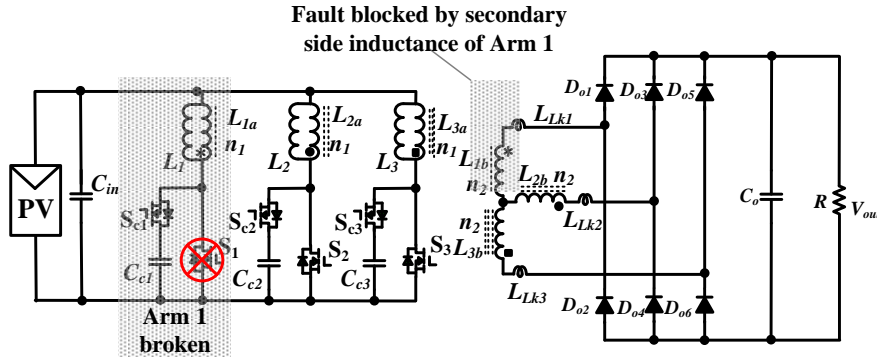
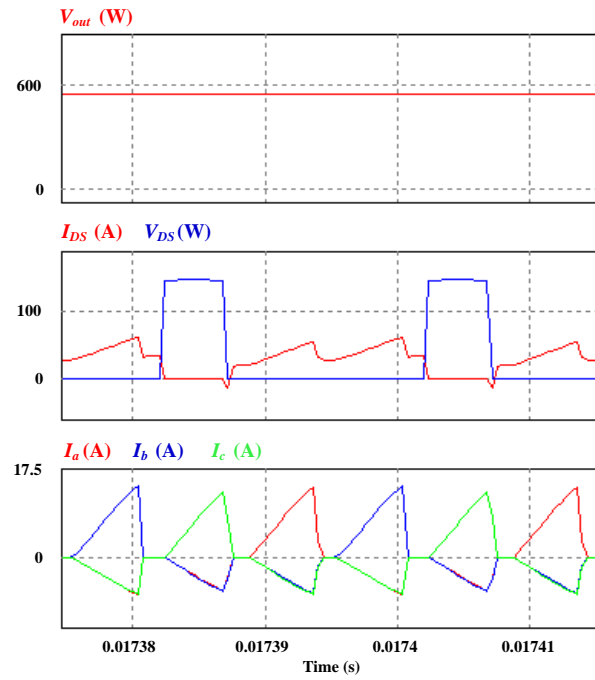
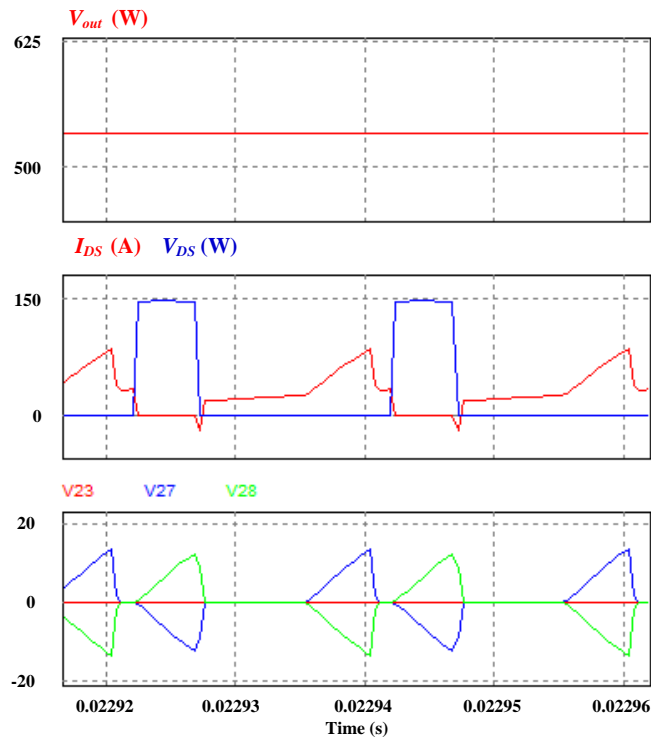


Fig. 11 Fault tolerance under a fault in the primary-side switching device.

Fig.12 presents the simulation results of a three-phase interleaved converter for PV applications. In order to avoid the shading influence, 12 250-W PV modules are connected in parallel. In the simulation, the switching frequency is 50 kHz and the turns ratio is 4. In this case, the PV output voltage (i.e. the converter input voltage) is low while the output current is high. By connecting with the proposed three-phase interleaved converter, the output voltage can be increased from 37 to 550 V. Fig. 12(a) and (b) are the simulation results for healthy condition and faulty condition, respectively. The soft switching can also be achieved, as shown in Fig. 12.



(a) Healthy operation



(b) Phase absence operation

Fig.12 Simulation results of the three-phase interleaved topology.

In order to improve power capacity, the proposed converter can be expanded with more bridge arms. In Fig. 13, the expandable characteristic is illustrated. The primary side can take more parallel bridge arms and the corresponding secondary side can add rectifier bridges to increase the system power. Owing to this modular structure, the power rating

can build up easily (e.g. over 10 kW).

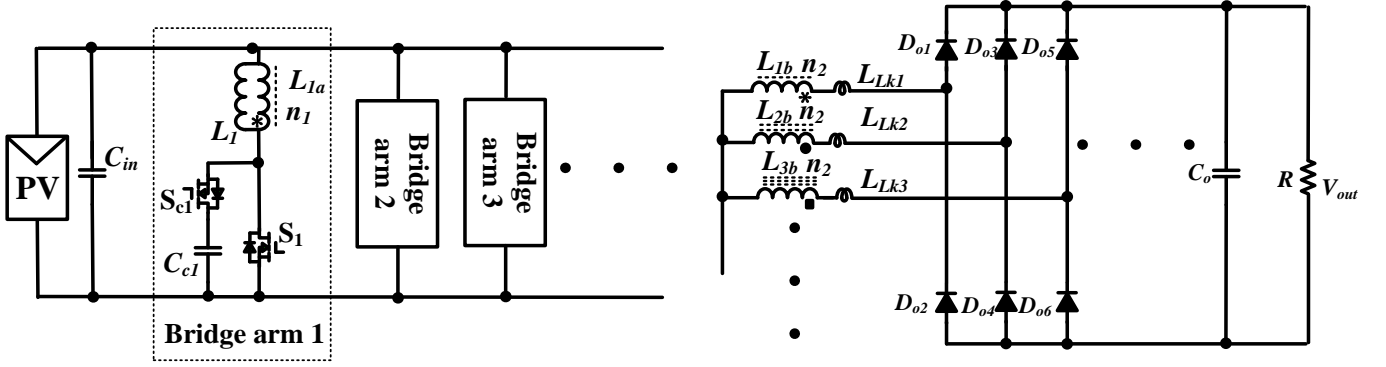


Fig. 12 Expandable characteristic of proposed converter.

In order to demonstrate the circuit advantages of the proposed converter, a detailed comparison with other converters is carried out and the results are presented in Table I. Compared with the three phase Weinberg converter in [24], the proposed converter has a lower main voltage stress and a lower switching loss due to the active clamp structure. The expandable characteristic and modular structure are also the merits of proposed converter. Compared with the full-bridge three-phase converter in [25], the proposed converter has less switching devices and can avoid the breakthrough of bridge arms. -

Table I. PERFORMANCE COMPARISON

Topology	Converter in [24]	Converter in [25]	Proposed converter
Numbers of active switches	3	12	6
Numbers of diodes	7	6	6
Voltage gain	$3ND/2$	<i>Phase shift control</i>	$N/(1-D)$
Voltage stress of active switches	$V_{in} + (N_T + N_L)V_o$	V_{in}	V_o/N
Voltage stress of output diodes	V_{out}	V_{out}	V_{out}
Input current ripple	Small	Small	Small
Output voltage ripple	Medium	Small	Small
Soft switching	No	Yes	Yes
Power capacity	Medium	Large	Large
Fault tolerance	Yes	Yes	Yes

Expandability	No	Yes	Yes
---------------	----	-----	-----

IV. EXPERIMENTAL VERIFICATION

An experimental platform was constructed and one arm prototype is shown in Fig 14. The main switches are of FDP047AN MOSFET with a switching frequency of 50 kHz. The coupled inductors use the Koolmu (0077109A7) magnetic cores with a turns ratio of 4, and the clamp capacitors are 4.7 μ F film capacitors. The input voltage is 5 V and the load is 25 Ω . Fig. 15(a)-(c) presents the output waveforms for the single-phase and three-phase inverters, which agree well with the theoretical analysis in Fig .6. In Fig. 15(a), it is noted that there is a 5-V voltage deviation caused by the leakage inductance of the coupled inductors; the primary side, two bridge arms have 90° phase shift angle, and the output pulse width can be controlled by phase shift angle. Fig. 15 (b) and (c) present the phase voltage waveforms and the line voltage waveforms of the three phase converter. The peak voltage of phase voltage is 42V, and the peak voltage of line voltage is 60V, in which the proportion relation of phase voltage and phase voltage is the same with the traditional three phase inverter. Fig. 15 (d)-(e) show the results for the four-phase inverter with a $T/4$ phase shift between phases. In Fig. 15 (e), the line voltage of V_{AD} and V_{CD} is different with V_{BD} , because the phase B has 180° phase shift angle with phase D; while phase C has 90° phase shift angle with phase D. Fig. 15 (f) presents the results of multi-level inverters with two winding pairs. The switching devices have the same duty ratio and phase shift as Fig. 9(b). It can be seen that the step wave is somewhat distorted by the leakage inductance but the peak voltage from the multi-level inverter is twice greater of a two-level inverter. Therefore, the multi-phase converter can achieve high power capacity with increase the phase number; the multi-level converter can achieve high voltage level with increase the phase number. Clearly, those experimental results have confirmed the effectiveness of the proposed bridge arm and the associated inverters. In this paper, only proof-of-concept study is deployed; with the development of high power level and high frequency switching devices, such as silicon carbon (SiC), the typical SiC devices QJD1210011_14 (1200V/100A) from *Powerex* can be employed in the proposed HFAC topology to realized high power level and frequency application.

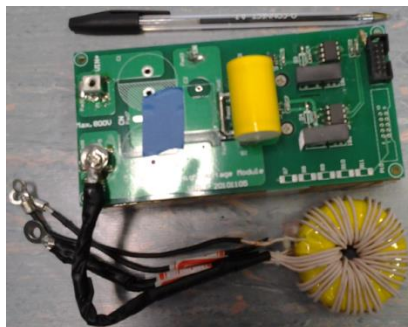


Fig. 14 Photograph of one converter arm.

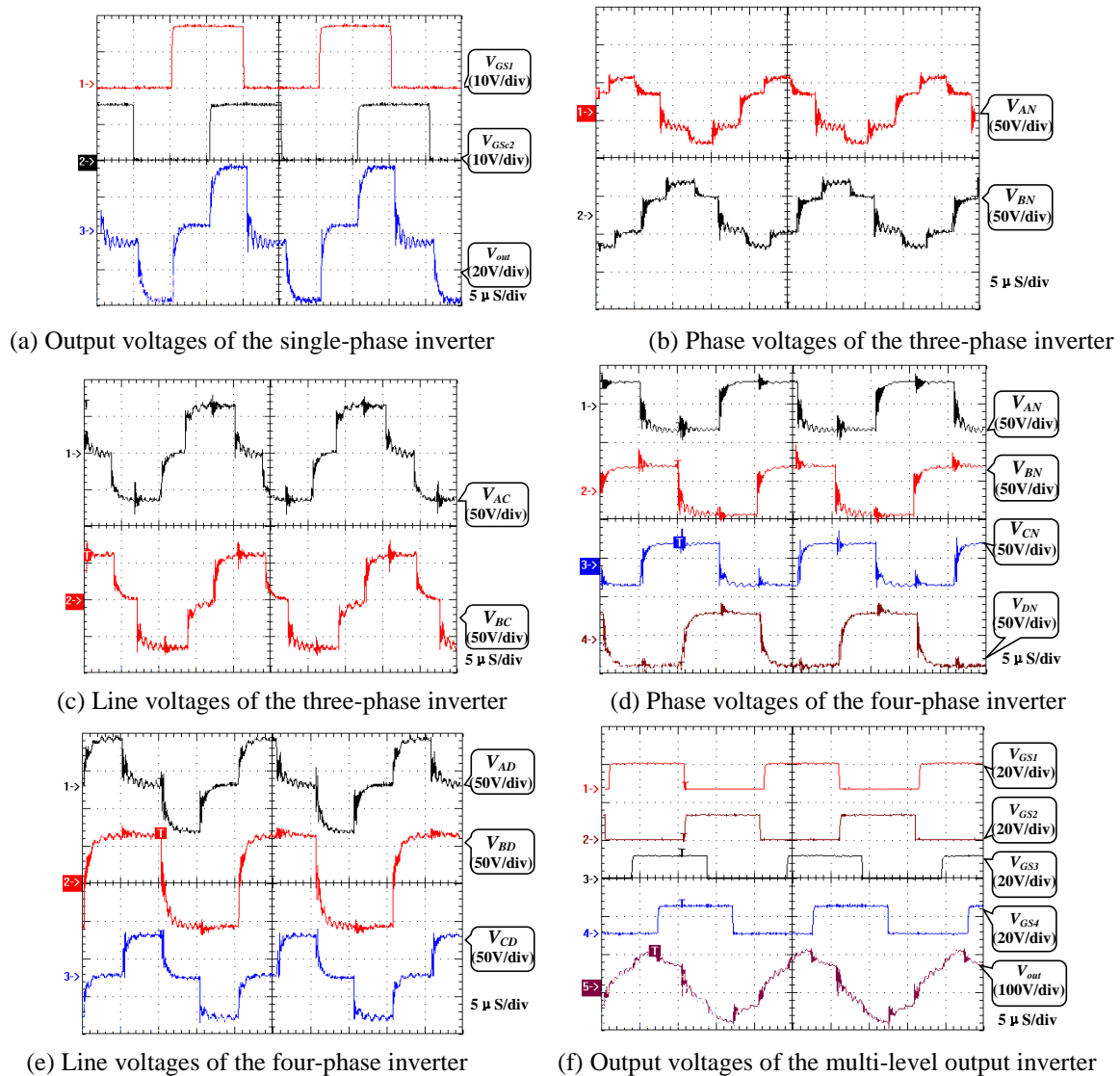


Fig. 15 Experimental results for the proposed inverters.

Fig. 16 shows the experimental results of a front-end DC-DC converter for PV applications. The input voltage is 10 V, the switching frequency is 40 kHz, the output voltage is 80V and the power rate is 400W. The soft switching of main switching devices can be achieved, as shown in Fig. 16(a). The voltage stress of the main switching devices is limited at a low level. The clamp switching devices also can realize soft switching. Fig. 16 (d) presents the input current and output voltage results and Fig. 16 (e) shows the efficiency curve. It can be seen that the maximum efficiency is 93.7% at 350 W, which is higher than the efficiency (92.5%) of a similar converter in [25].

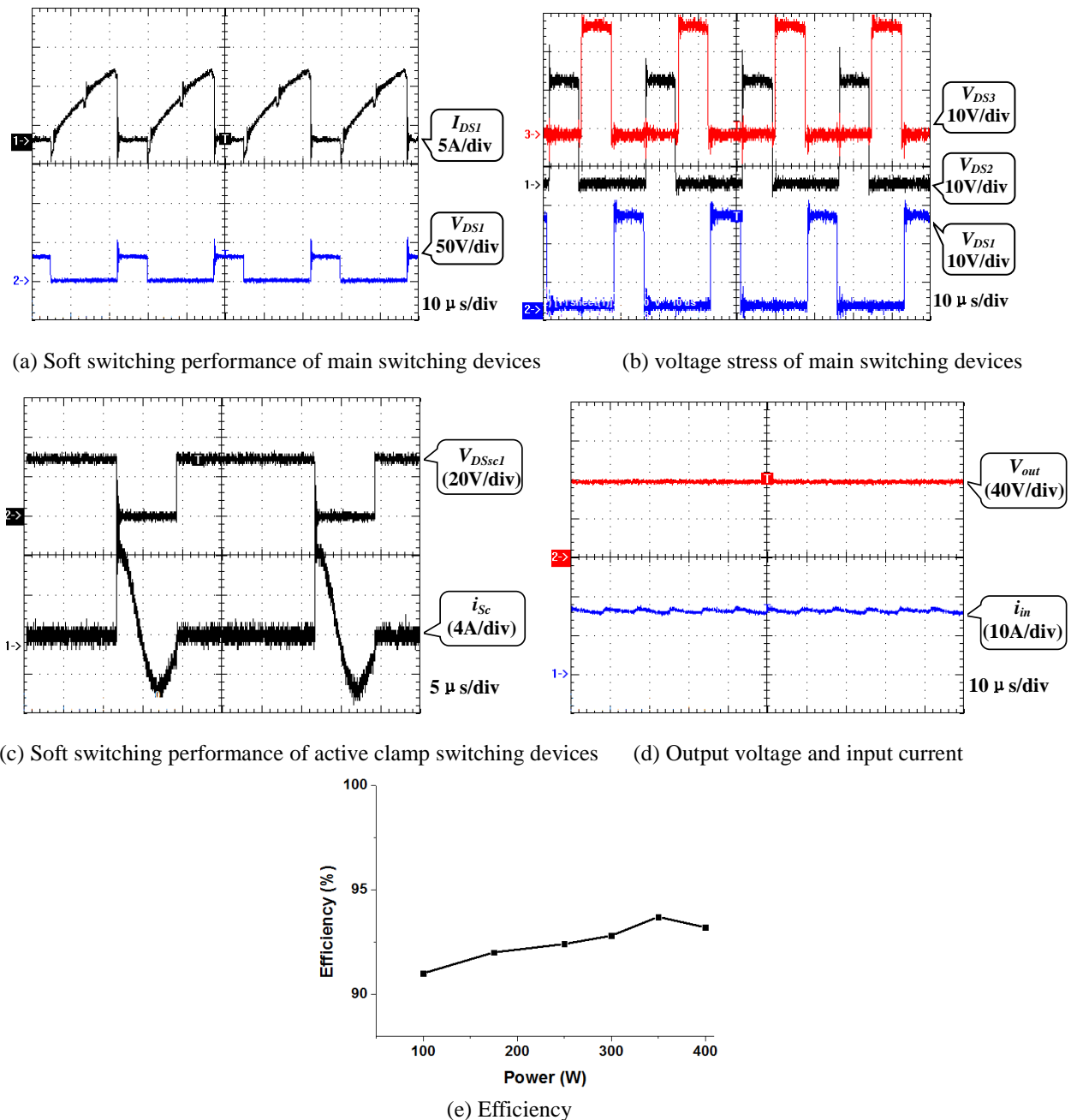


Fig. 16 Experiment results of the front-end DC-DC topology.

V. CONCLUSION

This paper has presented a group of novel high-frequency inverters integrated with the coupled inductor bridge. The coupled inductor bridge arm can provide electrical isolation and be built up to form single-phase, three-phase, multi-phase and multi-level inverters. Their modular and versatile features are particular useful for applications such as induction heating, DC-DC and AC-AC converters, wireless energy transfer and so forth. Based on the proposed topology, a front-end step-up DC-DC converter is developed for PVs as a demonstrator. Simulation and experimental results have validated the proposed topologies. They have improved performance than traditional inverters in terms of high flexibility for building multi-phase and/or multi-level inverters, and high-voltage high frequency output, low voltage stress and soft

switching capability, and isolated AC output. However, it needs to point out that this is a proof-of-concept research work at low voltage levels and its technology readiness level is between 2-3. In order to build up an application-ready product (TRL=9), it will take a long way and need significant industrial investment in the development work. Owing to the freedom of building phase and voltage levels, the proposed topology can potentially form **high power converters** that will then be used for **medium-voltage** applications.

References

- [1] B. Saha, and K. Rae-Young, "High Power Density Series Resonant Inverter Using an Auxiliary Switched Capacitor Cell for Induction Heating Applications," *IEEE Trans. Power Electronics*, vol. 29, no. 4, pp. 1909-1918, Apr. 2014.
- [2] F. S. Tsai, and F. C. Y. Lee, "High-frequency AC power distribution in Space Station," *IEEE Trans. Aerospace and Electronic Systems*, vol. 26, no. 2, pp. 239-253, Mar. 1990.
- [3] C. C. Antaloae, J. Marco, and N. D. Vaughan, "Feasibility of High-Frequency Alternating Current Power for Motor Auxiliary Loads in Vehicles," *IEEE Trans. Vehicular Technology*, vol. 60, no. 2, pp. 390-405, Feb. 2011.
- [4] S. Lourdes, S. Y. Ng, and P. C. K. Luk, "An alternative power grid - high frequency AC power distribution platforms." *IEEE 6th International Power Electronics and Motion Control Conference (IPEMC '09)*, 2009, pp. 1949-1956.
- [5] M. Sarhangzadeh, S. H. Hosseini, M. B. B. Sharifian, and G. B. Gharehpetian, "Multiinput Direct DC-AC Converter With High-Frequency Link for Clean Power-Generation Systems," *IEEE Trans. Power Electronics*, vol. 26, no. 6, pp. 1777-1789, Jun. 2011.
- [6] Z. Ye, P. K. Jain, and P. C. Sen, "Circulating Current Minimization in High-Frequency AC Power Distribution Architecture With Multiple Inverter Modules Operated in Parallel," *IEEE Trans. Industrial Electronics*, vol. 54, no. 5, pp. 2673-2687, Oct. 2007.
- [7] F. C. Lee, P. Barbosa, X. Peng, Z. Jindong, Y. Bo, and F. Canales, "Topologies and design considerations for distributed power system applications," *Proceedings of the IEEE*, vol. 89, no. 6, pp. 939-950, Jun. 2001.
- [8] Z. Ye, J. C. W. Lam, P. K. Jain, and P. C. Sen, "A Robust One-Cycle Controlled Full-Bridge Series-Parallel Resonant Inverter for a High-Frequency AC (HFAC) Distribution System," *IEEE Trans. Power Electronics*, vol. 22, no. 6, pp. 2331-2343, Nov. 2007.
- [9] P. Jain, M. Pahlevaninezhad, S. Pan, and J. Drobnik, "A Review of High-Frequency Power Distribution Systems: For Space, Telecommunication, and Computer Applications," *IEEE Trans. Power Electronics*, vol. 29, no. 8, pp. 3852-3863, Aug. 2014.
- [10] H. Wen, W. Xiao, and Z. Lu, "Current-Fed High Frequency AC Distributed Power System for Medium-High Voltage Gate Driving Applications," *IEEE Trans. Industrial Electronics*, vol. 60, no. 9, pp. 3736-3751, Sept. 2013.
- [11] R. O. Caceres, and I. Barbi, "A boost DC-AC converter: analysis, design, and experimentation," *IEEE Trans. Power Electronics*, vol. 14, no. 1, pp. 134-141, Jan. 1999.
- [12] B. Saha, K. Soon-Kurl, N. A. Ahmed, H. Omori, and M. Nakaoka, "Commercial Frequency AC to High Frequency AC Converter With Boost-Active Clamp Bridge Single Stage ZVS-PWM Inverter," *IEEE Trans. Power Electronics*, vol. 23, no. 1, pp. 412-419, Jan. 2008.
- [13] J. Liu, K. W. E. Cheng, and J. Zeng, "A Unified Phase-Shift Modulation for Optimized Synchronization of Parallel Resonant Inverters in High Frequency Power System," *IEEE Trans. Industrial Electronics*, vol. 61, no. 7, pp. 3232-3247, Jul. 2014.
- [14] C. Bernal, E. Oyarbide, P. M. Gaudo, and A. Mediano, "Dynamic Model of Class-E Inverter With Multifrequency Averaged Analysis," *IEEE Trans. Industrial Electronics*, vol. 59, no. 10, pp. 3737-3744, Oct. 2012.

- [15] M. Qiu, P. K. Jain, and H. Zhang, "An APWM resonant inverter topology for high frequency AC power distribution systems," *IEEE Trans. Power Electronics*, vol. 19, no. 1, pp. 121-129, Jan. 2004.
- [16] M. Qiu, P. K. Jain, and Z. Haibo, "Dynamic Performance of an APWM Resonant Inverter for High Frequency AC Power Distribution System," *IEEE Trans. Power Electronics*, vol. 21, no. 6, pp. 1556-1563, Nov. 2006.
- [17] Y. Zhou, W. Huang, P. Zhao, and J. Zhao, "A Transformerless Grid-Connected Photovoltaic System Based on the Coupled Inductor Single-Stage Boost Three-Phase Inverter," *IEEE Trans. Power Electronics*, vol. 29, no. 3, pp. 1041-1046, Mar. 2014.
- [18] W. Li, L. Fan, Y. Zhao, X. He, D. Xu, and B. Wu, "High-Step-Up and High-Efficiency Fuel-Cell Power-Generation System With Active-Clamp Flyback & Forward Converter," *IEEE Trans. Industrial Electronics*, vol. 59, no. 1, pp. 599-610, Jan. 2012.
- [19] S. H. Lee, K. T. Kim, J. M. Kwon, and B. H. Kwon, "Single-phase transformerless bi-directional inverter with high efficiency and low leakage current," *IET Power Electronics*, vol. 7, pp. 451-458, 2014.
- [20] M. E.-S. Ahmed, M. Orabi, and O. M. AbdelRahim, "Two-stage micro-grid inverter with high-voltage gain for photovoltaic applications," *IET Power Electronics*, 2013, Vol. 6, Iss. 9, pp. 1812-1821.
- [21] E. Koutroulis and F. Blaabjerg, "Methodology for the optimal design of transformerless grid-connected PV inverters," *IET Power Electronics*, 2012, Vol. 5, Iss. 8, pp. 1491-1499.
- [22] J.C. Rosas-Carol, J.M. Ramirez, F.Z. Peng, A. Valderrabano, "A DC-DC multilevel boost converter," *IET Power Electronics*, 2010, Vol. 3, Iss. 1, pp. 129-137.
- [23] B.L. Narasimharaju S.P. Dubey S.P. Singh, "Design and analysis of coupled inductor bidirectional DC-DC convertor for high-voltage diversity applications," *IET Power Electronics*, 2012, Vol. 5, Issue. 7, pp. 998-1007.
- [24] H.R.E. Larico and I. Barbi, "Three-Phase Weinberg Isolated DC-DC Converter: Analysis, Design, and Experimentation," *IEEE Trans. Ind. Electron.*, vol. 59, no.2, pp. 888 - 896, Feb. 2012.
- [25] C. Liu, A. Johnson, and J.-S. Lai, "A novel three-phase high-power soft-switched DC-DC converter for low voltage fuel cell applications," *IEEE Trans. Industry Applications*, vol. 41, no.6, pp. 1691-1697, Nov/Dec. 2005.